LA-UR- 11 - 03785

Approved for public release; distribution is unlimited.

Title: Unstable Richtmyer-Meshkov growth of solid and liquid metals in vacuum

Author(s): W. T. BUTTLER, D. M. ORO, D. L. PRESTON, K. O. MIKAELIAN, G. DIMONTE, F. J. CHERNE, R. S. HIXSON, C. MORRIS, J. B. STONE, G. TERRONES AND D. TUPA

Intended for: The Journal of Fluid Mechanics

Los Alamos
NATIONAL LABORATORY
EST. 1943

Los Alamos National Laboratory, an affirmative action/equal opportunity employer, is operated by the Los Alamos National Security, LLC for the National Nuclear Security Administration of the U.S. Department of Energy under contract DE-AC52-06NA25396. By acceptance of this article, the publisher recognizes that the U.S. Government retains a nonexclusive, royalty-free license to publish or reproduce the published form of this contribution, or to allow others to do so, for U.S. Government purposes. Los Alamos National Laboratory requests that the publisher identify this article as work performed under the auspices of the U.S. Department of Energy. Los Alamos National Laboratory strongly supports academic freedom and a researcher's right to publish; as an institution, however, the Laboratory does not endorse the viewpoint of a publication or guarantee its technical correctness.

Form 836 (7/06)

Unstable Richtmyer-Meshkov growth of solid and liquid metals in vacuum

W. T. BUTTLER[1]†, D. M. ORÓ,[1] D. L. PRESTON,[2] K. O. MIKAELIAN,[3] G. DIMONTE,[2] F. J. CHERNE,[4] R. S. HIXSON,[1] C. MORRIS,[1] J. B. STONE,[1] G. TERRONES[5] AND D. TUPA[1]

[1]Los Alamos National Laboratory, Physics, Los Alamos, NM 87544, USA
[2]Los Alamos National Laboratory, X-Computational Physics, Los Alamos, NM 87544, USA
[3]Lawrence Livermore National Laboratory, Physics, Livermore, CA 94550, USA
[4]Los Alamos National Laboratory, Shock & Detonation Physics, Los Alamos, NM 87544, USA
[5]Los Alamos National Laboratory, X-Theoretical Design, Los Alamos, NM 87544, USA

(Received ?; revised ?; accepted ?)

We present experimental results supporting physics based ejecta model development. Our present hypothesis assumes that ejecta form as a special limiting case of a Richtmyer-Meshkov (RM) instability where the Atwood number $A = -1$. From this assumption, we test established theory of spike and bubble growth rates related to the wavelength and amplitudes of surface perturbations through application of modern laser Doppler velocimetry techniques, which we apply in a novel manner to coincidentally measure bubble and spike velocities from explosively shocked solid and liquid metals. We also explore the link of ejecta formation from a solid material to the plastic flow stress it experiences at high-strain rates (10^7/s) and high strains (700%) as the fundamental link to the onset of ejecta formation. Our experimental observations allow us to bound the strength of Cu at the high strains and strain rates, revealing a unique diagnostic method for use at these extreme conditions. We also find inconsistencies between established bubble velocity theory and measurement.

1. Introduction

Los Alamos National Laboratory (LANL) is actively engaged in the development and implementation of ejecta source and transport models. The effort includes a broad array of theoretical and experimental activities, from flyer-plate and high-explosive (HE) driven ejecta source and transport measurements from machine roughened Sn surfaces (see Vogan et al. (2005); Buttler et al. (2007a,b); Zellner et al. (2007); Buttler & Zellner (2007); Zellner et al. (2008a,b,c); Zellner & Buttler (2008d)), to measurements presented here from surfaces with larger scale perturbations that permit the study of the physics of ejecta production with dynamic penetrating proton radiography (pRad).

There are at least two approaches to modeling *source term* ejecta dynamics. One commonly applied technique is to measure total mass-velocity distributions from a variety of surface finishes across a spectrum of shock breakout pressures, P_{SB}. Those measurements can then be integrated into a hydrodynamic-code that adds the measured source terms into the hydrodynamics when some critical condition is exceeded†. Such an empirical approach requires an extensive measurement basis, and often interpolation between

† Email address for correspondence: buttler@lanl.gov
† The transport of the ejecta in gasses also requires a model and some knowledge about

measurements if the surface features under consideration do not lie within the measured set. Complications to this approach include experimental observations that show that the total mass ejected, and the ejecta mass velocity distributions, sensitively link to the shockwave profile, e.g., whether the shockwaves are supported, as from flyer-plate type experiments, or unsupported, as from explosively driven shockwaves into metals (Buttler & Zellner 2011). Another approach is to evaluate and characterize materials according to their material properties and sensitivities to the initial driving conditions. Assuming a robust physics based model can be developed for a spectrum of interesting metals, then the parameter space of variables can be reduced. For example, at a minimum a viable model will accurately predict the total mass ejected, and a velocity distribution of the ejected mass based on the material and the geometry of the surface perturbations. It is this approach we are pursuing; and, because our experimental experiences have led us to the supposition that ejecta formation is characterized by a special limiting case of a Richtmyer-Meshkov (RM) instability (Richtmyer 1960; Meshkov 1969) where the Atwood number is $A = -1$ (Meyer & Blewett 1972), this approach allows a simple link of ejecta production to the surface perturbation's wavelengths and amplitudes.

2. Theoretical Motivation

Recent RM experiments at LANL explore ejecta physics around three features: total mass ejected, ejecta mass velocity distributions, and driving conditions under which ejecta do or do not form. The first two criteria for mass ejected from shocked metals at the metal-vacuum interface link to a liquid (*mostly* strength-less) RM instability model, while the final criterion links plastic unstable flow to materials with strength.

Considering the first two criteria (where $A = -1$) for metals that liquefy on shock or shock release, for the case that shockwaves are driven through a metal into sinusoidal perturbations machined onto the metal surface interfaced with vacuum, then when the shockwave arrives at the metal-vacuum interface it will first release to zero-pressure at the perturbation minimum and then reflect back into the metal as a rarefaction wave. A brief time later the shockwave releases to zero-pressure at the perturbation maximum, also reflecting back into the metal as a rarefaction wave. Under these conditions, strains produced by the shockwaves interacting with the perturbations and the vacuum interface causes the perturbation minimums to compress, invert, and then grow in tension as RM instabilities (spikes) into vacuum. Because the compressed RM spikes grow quickly relative to the initial perturbation maximums, the perturbation maximums invert and form bubbles that unstably grow into the metal causing metal to flow into the spikes to support the spike growth. In this picture, bubbles and spikes refer to peak penetration depths on the two opposite sides of the "free-surface," which is nominally defined as the initial zero amplitude of the sinusoidal perturbations, e.g., the initial surface sinusoidal perturbation can be defined as $\eta(x) = \eta_0 \sin(kx)$, where the wavenumber $k = 2\pi/\lambda$, λ is the perturbation wavelength, x is the planar (xz) dimension parallel to the "free-surface" and incident shockwave, and η_0 is the initial perturbation amplitude oriented parallel to the vertical dimension (y-axis) orthogonal to the xz-plane. In this two-dimensional geometry the literature usually takes $\eta(x,t)$ positive into the metal, and $-\eta(x,t)$ into the vacuum. With this definition, we define $\dot{\eta}^{b,s}(x,t)$ as the velocities of the bubbles (spikes) relative to the free surface velocity u_{fs} – in the laboratory frame we directly measure with laser Doppler velocimetry (LDV) u_{fs}, $u_b^\infty = u_{fs} - \dot{\eta}^b$, and $u_s^\infty = u_{fs} + |\dot{\eta}^s|$, e.g.,

the ejecta particle sizes and mass distributions within the ejecta cloud. We are presently not diagnosing well the ejecta particles sizes or their velocity distributions.

see Yeh & Cummins (1964); Forman, George & Lewis (1965a,b); Buttler, et al. (2004); Strand, et al. (2006).

We shall use the linear theory developed in Richtmyer (1960) to describe the extremely short, early time evolution of the perturbations as the perturbations compress when they pass through zero during the inversion process. For the subsequent period of substantial growth (more than thirty fold) we use a nonlinear model developed in Mikaelian (1998) to describe the evolution of bubbles and spikes relative to the free surface.

Setting $g = \eta_0 k = 0$ in Eq. 5a in Mikaelian (1998), gives

$$\frac{\dot{\eta}}{\dot{\eta}_0} = \frac{\mathcal{Y}_0}{\mathcal{Y}} = \sqrt{\frac{3}{2}}\frac{1}{\mathcal{Y}} = \sqrt{\frac{3}{2}}\frac{1}{\sqrt{e^{3\eta k} + 1/2}}, \tag{2.1}$$

where $\mathcal{Y}^2 = e^{3\eta k} + 1/2$. This equation applies to both bubbles and spikes provided we take η and $\dot{\eta}$ positive (negative) for bubbles (spikes). Equation 2.1 relates the bubble or spike velocity $\dot{\eta}^{b,s}$ to its amplitude $\eta^{b,s}$, and its initial growth rate $\dot{\eta}_0$, which we now describe.

Integrating Eq. 2.1 gives

$$\begin{aligned}\dot{\eta}_0 k\, t &= \frac{2\sqrt{2}}{3\sqrt{3}}\mathcal{Y} - \frac{2}{3} + \frac{1}{3\sqrt{3}}\ln\left[\frac{(\sqrt{3}+1)(\sqrt{2}\mathcal{Y}-1)}{(\sqrt{3}-1)(\sqrt{2}\mathcal{Y}+1)}\right] \\ &= \frac{2\sqrt{2}}{3\sqrt{3}}\mathcal{Y} - \frac{2}{3} + \frac{\eta k}{\sqrt{3}} + \frac{1}{3\sqrt{3}}\ln\left[\frac{\sqrt{3}+1}{(\sqrt{3}-1)(\sqrt{2}\mathcal{Y}+1)^2}\right],\end{aligned} \tag{2.2}$$

which is equivalent to Eq. 11 in Mikaelian (1998) with $\eta_0 k = 0$, and Eq. 36 in Mikaelian (2010); a form of this equation was first presented in Zhang (1998).

The asymptotic spike velocity can be approximated from either Eq. 2.1 or 2.2 by evaluating both equations as $\eta^s \to -\infty$. For Eq. 2.2, the terms must be rearranged, but from Eq. 2.1 we find

$$\lim_{\eta\to-\infty} \dot{\eta}(\eta) = \sqrt{3}\dot{\eta}_0^s, \tag{2.3}$$

which is the maximum velocity attainable by the spikes in theis model.

An approximation to the bubble velocity in Eq. 2.1 is given as Eq. 17 in Mikaelian (1998)

$$\begin{aligned}\dot{\eta}_t^b &= \frac{2\dot{\eta}_0^b}{2 + 3\dot{\eta}_0^b k t} \\ \Rightarrow \dot{\eta}_\infty^b &\equiv \lim_{t\to\infty} = \frac{2}{3kt}.\end{aligned} \tag{2.4}$$

The asymptotic limit applies at very late times and is independent of the initial perturbation amplitudes.

Equations 2.1, 2.2, 2.3 and 2.4 require the initial growth rates $\dot{\eta}_0^{b,s}$. For shockwave driven incompressible linear instability growth ($\eta_0 k \ll 1$)

$$\dot{\eta}_0^b = -\dot{\eta}_0^s = \eta_0 k u_{fs}, \tag{2.5}$$

as shown by Richtmyer (1960). This result is modified by two effects: compressibility and nonlinearity. Richtmyer showed that to account for compressibility one should use not the preshock amplitude η_0 but the postshock, compressed amplitude $\eta_0(1 - u_{fs}/u_{sh})$, where u_{sh} is the shockwave speed in the metal caused by the loading stress P_{SB} just prior to the arrival of the shockwave at the free-surface. While Richtmyer investigated the case of a shockwave moving from a low- to a high-density fluid, for the opposite case

Meyer & Blewett (1972) found that using the average of the preshock and postshock amplitudes gave better agreement with direct numerical simulations. Hence we use

$$F_{cmp} = 1 - \frac{u_{fs}}{2u_{sh}} \tag{2.6}$$

as the compression factor. These prescriptions were developed for linear amplitudes and therefore the compression factor is the same for both bubbles and spikes, i.e., $F^b_{cmp} = F^s_{cmp} = F_{cmp}$.

In the nonlinear regime – the linear conditions are not met – a second nonlinearity factor F_{nl} differentiates between bubbles and spikes. Velikovich & Dimonte (1996) addressed the nonlinear regime with a perturbation model and a series of simulations of bubble and spike growth. Later, Dimonte & Ramaprabhu (2010) provided a nonlinear factor as a fit to the spike simulations in Velikovich & Dimonte (1996):

$$F^s_{nl} = \frac{1}{1 + (\frac{\eta_0 k}{2})^2}. \tag{2.7}$$

A similar fit to the bubble amplitudes gives a nonlinear bubble factor:

$$F^b_{nl} = \frac{1}{1 + \frac{\eta_0 k}{6}}. \tag{2.8}$$

Assuming that the effects of compressibility and nonlinearity act independently we obtain

$$|\dot{\eta}^{b,s}_0| = F_{cmp} F^{b,s}_{nl} |\eta_0 k u_{fs}|. \tag{2.9}$$

The third criterion we explore evaluates whether ejecta formation is more fundamental than a simple link to the material phase at the time of shock or shock release at the metal-vacuum interface, i.e., are the criteria of ejecta formation fundamentally linked to basic material properties such as material yield strength at the strains and strain rates in the material as experienced in the interaction of shock induced stresses and the perturbation geometry. If this last hypothesis is correct, then it is possible to form ejecta even when the material is solid on shock and shock release. This hypothesis centers on an interesting result in Piriz, Lopez-Cela & Tahir (2010), where, for our purposes, we modify their result and relate the spike amplitude η^s_∞ for materials with strength to the initial density of the material ρ_0, η_0, P_{SB}, k, and u_{fs} (e.g., see Eq. 3 in Piriz, Lopez-Cela & Tahir (2010)):

$$\frac{\eta^s_\infty - \eta_0}{\eta_0} \approx 0.29\eta_0 k \frac{\rho_0 u^2_{fs}}{Y}, \tag{2.10}$$

where Y must be the mean flow stress of the material at high strains and high strain rates – not the elastic-plastic yield assumed in Piriz, Lopez-Cela & Tahir (2010). We explore this property in shock stress regimes where the material is solid on shock and release, with $A = -1$, in contrast with the Piriz study where $A \approx 1$. There are other key differences between the what we will refer to as the Piriz model and these experiments. For example, the Piriz model assumes that $\dot{\eta}^s \equiv \dot{\eta}^b$, which is true for $A = 1$ study – our $A = -1$ situation releases to zero pressure and the spike and bubble velocities and heights are quite different from each other. Importantly we note that the Piriz model links to no constitutive material properties. Nevertheless, it is a relevant idea and approach, and it was the motivation behind our interest in solid material RM studies.

3. Experimental approach

The path by which we arrived at our present experimental approaches to explore the physics described by Eqs. 2.1 to 2.10 began with small scale HE and flyer-plate experiments on roughened surfaces (Vogan et al. 2005; Zellner et al. 2007). From those studies it was concluded that the geometries of most interest centered on one-dimensional (1D) HE driven experiments. The 1D approach led naturally to use of HE lenses combined with boosters to smooth out the drive as the shockwave releases to zero pressure as it arrives at the vacuum-metal interface. Also, because of our successes with the smaller scale experimental studies, we began pRad work with larger scale perturbations that were imageable at the pRad facility. Within our second year of pRad work the best designs began to emerge, with the requirements to support the ejecta model development efforts being the smallest resolvable features – wavelengths and amplitudes – at the pRad facility with $\times 3$ magnification, combined with uniaxial 1D drives.

In designing packages that addressed the full set of needs we settled on a P076 (76 mm diameter HE lens) and we evaluated two different HE boosters: TNT and PBX 9502. These HE geometries required experimental hydrodynamic proof and were tested by fielding two hydro tests that were identical except for the two different booster systems. Otherwise, the two hydro tests fielded 10 mm of Sn in contact with 2 mm of Ti that was in contact with the HE booster, similar to the designs seen in Fig. 1. We also incorporated momentum trapping on the tests (see Bourne & Gray (2005a,b)).

Hydrodynamic simulations of the TNT geometry with Sn targets predicted $P_{SB} < 19$ GPa. However, the experimental hydro-tests reached $P_{SB} \approx 28$ GPa for the PBX 9502 booster, and $P_{SB} \approx 24.5$ GPa for the TNT booster – again the samples were Sn of height 10 mm. Because of the high loading pressures we modified our experimental geometry further to include a right cylinder Calcitol booster of diameter 76 mm and height 16 mm together with the P076 HE lens for the Sn target experiments. Hydrodynamic simulations of the Calcitol geometry with the 2 mm Ti buffer and 4 mm Sn target predicted Sn pressures of $P_{SB} < 16$ GPa. However, because of continuing concerns that Sn experiments would not be solid-on-release† with the lenses and Calcitol boosters, we also designed a Cu package that used a 76 mm diameter by 10 mm tall right cylinder PBX 9501 booster, for which we were certain that the Cu would be solid upon release to zero pressure. Our concerns were well founded as the first pRad Sn experiment (Sn-pRad0425) was observed to reach peak stresses of $P_{SB} \approx 27$ GPa. Therefore, we next fielded the Cu target (Cu-pRad0426) which was observed to reach peak stresses of $P_{SB} \approx 36$ GPa, which is clearly solid on shock and release. Lastly, we added a 10 mm thick Sn cylinder between the Calcitol and the Ti, and that experiment (Sn-pRad0427) was observed to drop to $P_{SB} \approx 22$ GPa, still above melt on release for Sn. Figure 1 illustrates the experimental geometries for the three FY10 RM instability experiments, and Fig. 2 presents selected pRad data.

4. Experimental Data and Discussion

If Eq. 2.10 captures the physics relevant to RM instability growth in solids with $A = -1$, then the dynamics predicted for a target that is solid on release, assuming the perturbation wavenumbers are well chosen, are that at least one perturbation region will grow without bound, another perturbation region will not grow at all (its velocimetry

† The Sn samples are shocked along the Hugoniot to pressures where the Sn shocks from the solid β to the solid body-centered-tetragonal (BCT) phase and then releases to a mixed solid-liquid phase.

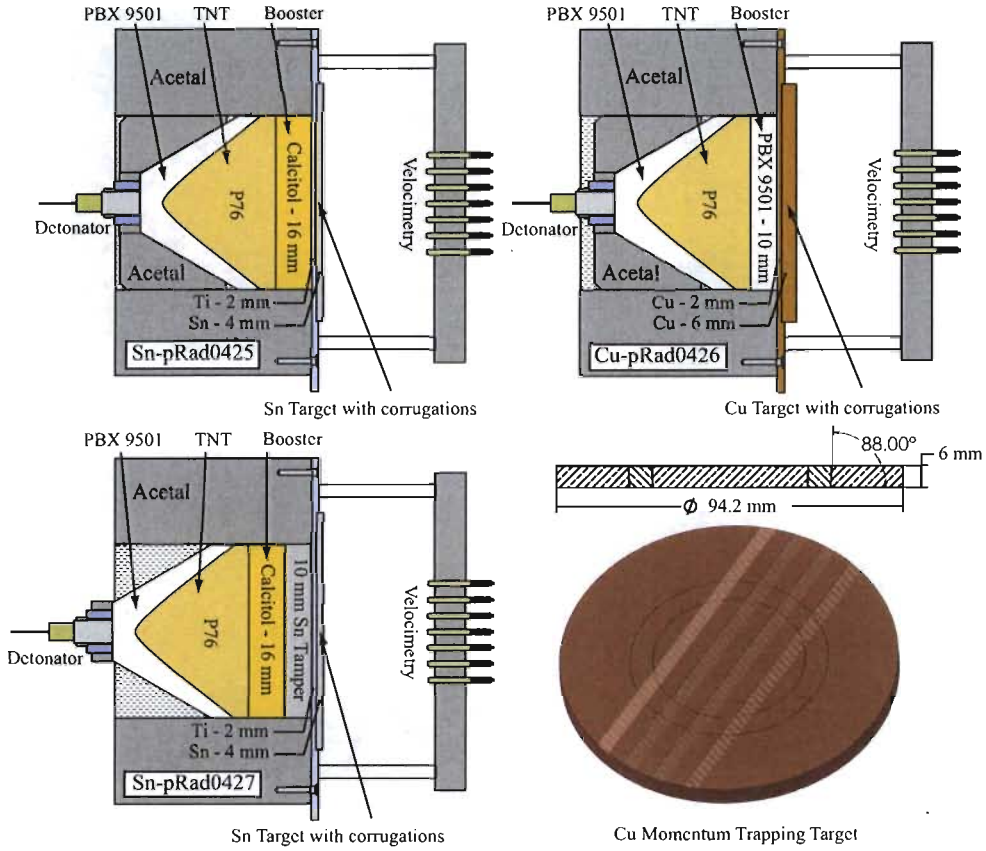

FIGURE 1. pRad RM experimental package geometries encase in acetal plastic a 76 mm diameter plane-wave HE lens used to uniformly detonate a HE booster cylinder in contact with a buffer plate; the sample/target is mounted to the buffer plate atop the acetal plastic as well. The target design incorporates momentum trapping concepts (Bourne & Gray 2005a,b), as illustrated on the lower right together with the target perturbation schemes. The targets were machined to a diamond turn finish that included four bands of sinusoidal corrugations, of $\lambda = 550$ μm wavelength and varying amplitudes (see Fig. 2). Each corrugation band was eight wavelengths wide and separated by flat regions that were 5 mm wide. Over each corrugation band and intervening flat region was positioned a velocimetry probe used to measure jump times and velocity histories over the duration of the experiment.

would be indistinguishable from u_{fs}), and that at least one of the remaining perturbation regions will present with initial plastic RM growth that quickly arrested; these are the dynamics observed in the Cu experiment, but because the two Sn experiments released to a partial liquid phase they of course grew without bound. Nevertheless, the Sn data help validate the ejecta mass and the ejecta mass velocity distributions.

Figure 2 shows one late time image from each of the three pRad experiments illustrated in Fig. 1: experiment Sn-pRad0425 is to the left (Sn at $P_{SB} = 26.7$ GPa), Sn-pRad0427 is in the center (Sn at $P_{SB} = 21.9$ GPa), and Cu-pRad0426 is to the right (Cu at $P_{SB} = 36.1$ GPa). For the Sn experiments the time at which the image was captured relative to breakout of the shockwave at the metal-vacuum interface was $\Delta t \approx 7.9$ μs, and for the Cu experiment $\Delta t \approx 7.8$ μs. The free-surface velocities u_{fs} were measured

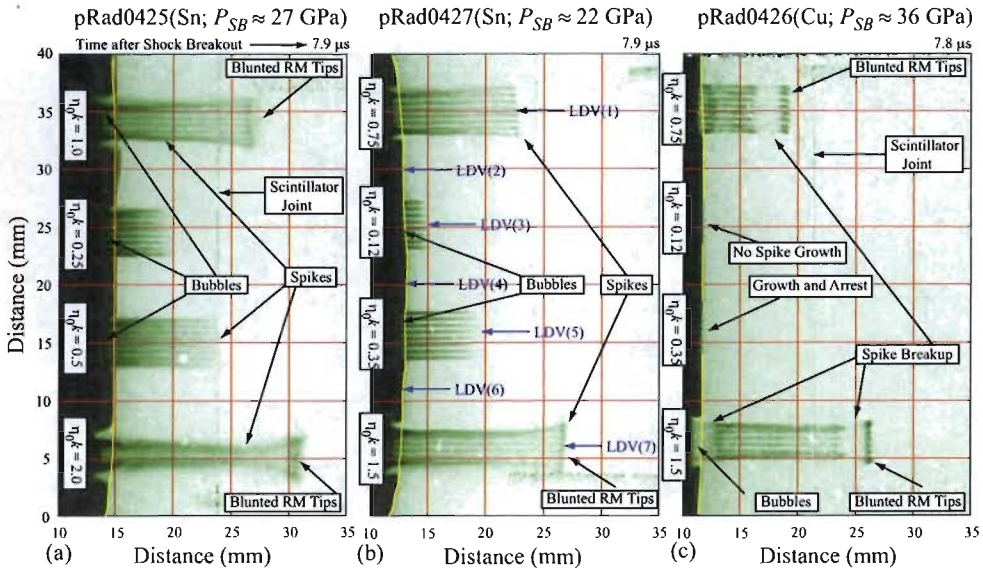

FIGURE 2. FY10 pRad images. Sn is to the left (a) and in the center (b), and Cu is to the right (c). The image time relative to shockwave breakout at the vacuum-metal interface is to the right just above each image. The wavelength of the perturbations was $\lambda = 550$ μm, and the initial wavenumber and amplitude product $\eta_0 k$ for each perturbation region is shown to the left of each perturbation region. The free surface is nominally outlined in yellow, and u_{fs} was diagnosed with laser Doppler velocimetry (LDV) from the flat regions between each perturbation region. Bubbles and spikes are noted on the figures. LDV locations are noted in blue within (b).

with LDV from the flat areas between each perturbation region, and the bubble and spike velocities were measured by LDV as well.

The asymptotic Sn spike-velocity u_s^∞ for each unstable spike seen to grow can be approximated as the nominal height of the spikes seen on the Fig. 2 grids divided by Δt, and u_{fs} can be estimated in like manner.

The free-surface in Cu-pRad0426 experiment remains the flattest at late times, with Sn-pRad0425 the next flattest, but nevertheless showing some later time edge-release effects even though the idea of momentum trapping is to isolate the center disk, as shown in Fig. 1, from side rarefaction wave effects. The center image of Sn-pRad0427 is the most polluted by edge release effects, but on that experiment we added the 10 mm tall right Sn cylinder between the Calcitol booster and the Ti surface, as seen in Fig. 1, so this result is expected.

When a shocked surface is liquid-on-shock and -release, or liquid-on-release, the velocimetry is generally unremarkable. In such a liquid release state, assuming velocimetry measurements return results, the free-surface velocity is seen to jump from zero velocity to a high velocity and then hold steady at that velocity because it is liquid and retains no residual material strength greater than the residual surface tension, i.e., the shocked surface is for all intents and purposes a free-particle traveling at $u_{fs}^\infty = Const.$ Because the two Sn experiments (Sn-pRad0425 and Sn-pRad0427) were shocked to $P_{SB} \gtrsim 22$ GPa, the Sn velocimetry falls within this category: an unremarkable result that shows only asymptotic bubble, spike, and free-surface velocities – u_b, u_s^∞, and u_{fs}, respectively†.

† Without loss of generality, within the text we alternately refer to u_{fs} and u_{fs}^∞, which are equivalent late time constant velocities we measure with LDV.

	$\eta_0 k$	η_0 (μm)	τ^s_{bo} (μs)	τ^s_{rt} (μs)	$\dot{\eta}^{b,m}_{t=0.3\ \mu s}$ (mm/μs)	$\dot{\eta}^{b}_{t=0.3\ \mu s}$ (mm/μs)	$\dot{\eta}^{s,m}_{\infty}$ (mm/μs)	$\dot{\eta}^{s}_{\infty}$
Sn-pRad0425	0.25	22	14.441	< 0.14	−0.07	−0.12	0.63	0.61
$P_{SB} = 26.7$ GPa	0.5	44	14.431	< 0.13	−0.15	−0.15	1.14	1.16
$\langle u^{\infty}_{fs}\rangle = 1.85$ (mm/μs)	1.0	88	14.430	< 0.21	−0.14	−0.17	1.60	1.97
$u_{sh} = 3.97$ (mm/μs)	2.0	175	14.365	< 0.34	−0.26	−0.18	2.10	2.46
Sn-pRad0427	0.12	11	17.289	< 0.11	0.00	−0.08	0.31	0.26
$P_{SB} = 21.9$ GPa	0.35	31	17.266	< 0.09	−0.02	−0.13	0.81	0.74
$\langle u^{\infty}_{fs}\rangle = 1.59$ (mm/μs)	0.75	66	17.253	< 0.08	−0.09	−0.16	1.26	1.43
$u_{sh} = 3.77$ (mm/μs)	1.5	131	17.206	< 0.22	−0.06	−0.17	1.78	2.09

TABLE 1. Tin RM instability velocimetry from Sn-pRad0425 and Sn-pRad0427. $\lambda = 0.55$ mm; η_0: initial perturbation amplitude; τ^s_{bo}: time the spikes began to compress and invert from their initial minimums; τ^s_{rt}: time over which the spikes rise to 90% of their maximum velocity; $\dot{\eta}^{b,m}_{\infty}\langle 0.3$ μs): bubble velocity relative to u_{fs} at $t = 0.3$ μs, $\dot{\eta}^{s,m}_{\infty}$ the measured asymptotic spike velocity; $\dot{\eta}^{s}_{\infty}$: the predicted spike velocity. The uncertainty in *all* measured velocities is of $O(0.01$ to 0.02 mm/μs), and the uncertainties in τ^s_{bo} is of $O(0.005$ μs$\rangle$.

Therefore, for the Sn experiments we simply tabulate the observed quantities of interest, such as P_{SB} (which is calculated from the measured u_{fs}) and the shock velocity u_{sh} in the material at P_{SB}, which is used to calculate the predicted spike and bubble velocities $\dot{\eta}^{s}_{\infty}$ and $\dot{\eta}^{b}_{\infty}$ that are compared with the measured spike and bubble velocities $\dot{\eta}^{s,m}_{\infty}$ and $\dot{\eta}^{b,m}$ in table 1.

Regarding the Sn results reported in table 1, P_{SB} listed in the details (first) column is estimated from $\langle u_{fs}\rangle$, which is the average of the three u_{fs} measurements (LDV probes 2, 4, and 6) from the flat surfaces between the four perturbation regions, and the shock velocity u_{sh} in the metal is calculated from $\langle u_{fs}\rangle$ as well†. The uncertainty in $\langle u_{fs}\rangle$ is on the order of 0.01 to 0.02 mm/μs. The spike and bubble velocities ($\dot{\eta}^{s,m}_{\infty}$ and $\dot{\eta}^{b,m}$) were coincidentally measured with a single LDV probe‡ above each perturbation region (LDV probes 1, 3, 5, and 7). The early time bubble dynamics are not well resolved, possibly due to noise, but the late time measured bubble velocities $\dot{\eta}^{b,m}$ are reported (in a negative sense) relative to $\langle u_{fs}\rangle$. In table 1 we also report t^s_{bo}, the time of shock-breakout time relative to CVR¶ at the minimum perturbation heights, and t^s_{rt}, the measured time over which the spikes are observed to rise to 90% of their asymptotic velocity $\dot{\eta}^{s,m}_{\infty}$. The uncertainty in these time values is on the order of 0.005 μs. The earliest motion should first occur in the perturbation regions with the largest amplitude for a 1D-HE drive and that is what was observed.

The Cu velocimetry is more interesting because the Cu is solid-on-shock and shock-release, and it is expected that some spikes will exhibit unconstrained growth of solid material, and some will exhibit no growth, while some will exhibit initial growth that is arrested. While the Cu data on the right in Fig. 2 appears to present these predicted phenomena, the result is only qualitative in appearance. However, the Cu velocimetry presented in Fig. 3 quantifies the remarkable prediction. For example, for the largest wavenumber and amplitude product, the spike growth appears to be unconstrained; if there is a sharp spike velocity jump followed by a release to a lower velocity for the

† We calculate P_{SB} and u_{sh} using standard impedance matching techniques.

‡ The LDV spot size is ≈ 1 mm, and $\lambda = 0.55$ mm, allowing coincident measurement of both the bubble and spike velocities.

¶ CVR relates the time high voltage is dumped to the detonators that initiate the HE lens.

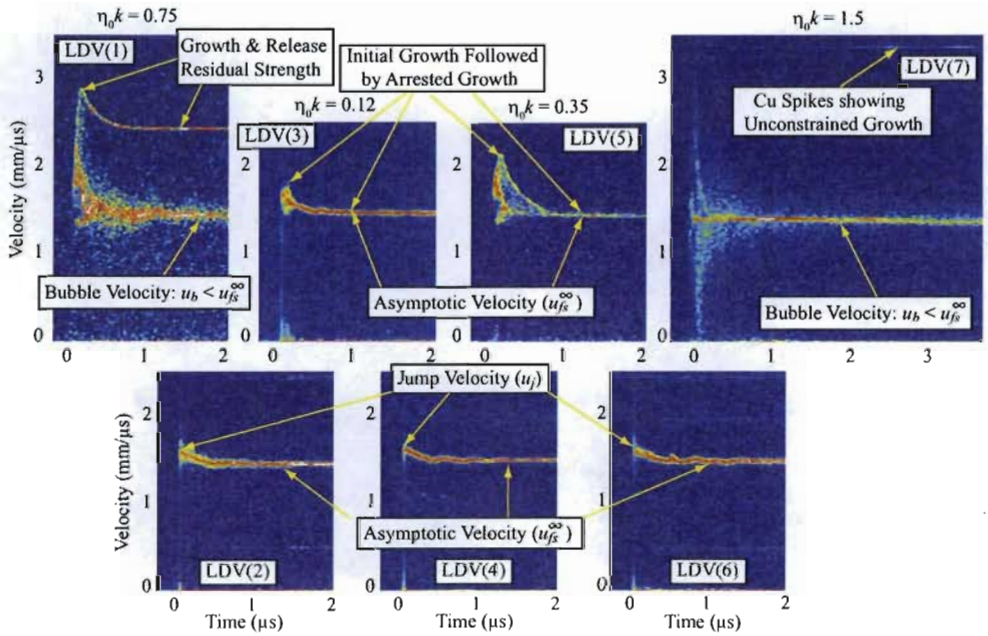

FIGURE 3. Velocimetry measured by the LDV probes for Cu-pRad0426. The upper four panels show the velocities from the 4 regions with corrugations and are labeled by $\eta_0 k$. The lower three panels show the velocities from the intervening flat regions. For $\eta_0 k = 1.5$ and 0.75 the asymptotic spike velocity and bubble velocity are clearly visible. For $\eta_0 k = 0.75$ the velocity relaxation to the peak value u_{pk}^{S} indicates that material strength is affecting spike growth rates. Obviously for $\eta_0 k = 0.35$, and upon close examination for $\eta_0 k = 0.12$, u_{pk}^{s} is larger than the peak free-surface velocity and releases down to u_{fs}^{∞} indicating initial growth of the perturbations that is subsequently completely arrested.

$\eta_0 k = 1.5$ perturbations it is not resolved in the velocimetry. Either way, for the largest amplitude Cu perturbations it appears as if the spikes grew quickly and then broke up, according to the penetrating proton radiography. In contrast, for the $\eta_0 k = 0.75$ perturbation region the spikes accelerate to a high velocity and then quickly decelerate to a lower asymptotic velocity $u_s^{\infty} = Const > u_j > u_{fs}^{\infty}$, where u_j is the maximum measured u_{fs} which is greater than the late-time asymptotic free-surface velocity u_{fs}^{∞} of the solid Cu. From the Fig. 2 radiography these $\eta_0 k = 0.75$ spikes also appear to have broken up. The final two regions present the most interesting phenomena in that it appears in the velocimetry that both perturbations initially grew but then the growth quickly arrested and the spike velocities decayed to $u_{\infty}^{s,m} = u_{fs}^{\infty} < u_j$. The average jump velocity $\langle u_j \rangle$ is the average of the LDV measurements in the three flat regions (probes 2, 4, and 6) between the perturbation regions and is used to estimate P_{SB} and u_{sh} for the Cu, as usual. After shock breakout, u_j releases down to a lower u_{fs}^{∞} as the Cu reverberates with the release waves reflecting through the Cu sample. This is typical velocimetry from materials with strength.

It is interesting, if not unexpected, that Eq. 2.3 predicts well the measured peak velocities $\dot{\eta}_{pk}^{s}$ for the Cu spike growth – for both cases where the spikes breakup after plastic growth, and when the spike growth arrests. This interesting result may be simply related to the RM physics predicting the driving impulse. In the Cu case the spikes breakup when the flow stress is exceeded in plastic deformation at high strains and high strain rates, leading to constant $u_{\infty}^{s} > u_{fs}^{\infty}$, similar to the liquid Sn spikes. In the situation that

Cu-pRad0426	$\eta_0 k$	η_0 (μm)	τ^s_{bo} (μs)	τ^s_{rt} (μs)	$\dot{\eta}^{b,m}_{t=0.3\ \mu s}$ (mm/μs)	$\dot{\eta}^{s,m}_{\infty}$ (mm/μs)	$\dot{\eta}^{s}_{pk}$ (mm/μs)	$\dot{\eta}^{s}_{\infty}$ (mm/μs)
$P_{SB} = 36.1$ GPa	0.12	11	13.189	< 0.08	0.00	0.00	0.17	0.15
$\langle u_j \rangle \approx 1.58$ (mm/μs)	0.35	31	13.187	< 0.08	0.00	0.00	0.57	0.43
$\langle u^{\infty}_{fs} \rangle \approx 1.46$ (mm/μs)	0.75	66	13.170	< 0.09	-0.02	0.98	1.30	0.82
$u_{sh} = 5.12$ (mm/μs)	1.5	131	13.150	?	-0.02	1.89	1.82	1.20

TABLE 2. Copper RM instability velocimetry from Cu-pRad0426 ($\lambda = 0.55$ mm) η_0: initial perturbation amplitude; τ^s_{bo}: time the spikes began to compress and invert from their initial minimums; τ^s_{rt}: time over which the spikes rise to 90% of their maximum velocity; $\dot{\eta}^{b,m}_{\infty}\langle 0.3\ \mu s)$: bubble velocity relative to u^{∞}_{fs} at $t = 0.3\ \mu$s, $\dot{\eta}^{s,m}_{\infty}$ the measured asymptotic spike velocity; $\dot{\eta}^{s}_{\infty}$: the predicted spike velocity. The uncertainty in *all* measured velocities is of $O(0.01$ to 0.02 mm/μs), and the uncertainties in τ^s_{bo} is of $O(0.005\ \mu s)$.

the Cu spike growth begins and then is arrested, the driving impulse is still predicted by the RM physics, but because the flow stress is not exceeded the spike growth is arrested and $u^s_{\infty} = u^{\infty}_{fs}$. The Cu velocimetry details are tabulated in table 2.

We can also review how well Eq. 2.4 predicts $\dot{\eta}^b$ at early and late times, for at least the Sn experiments. While the model implies that the relative difference between u^{∞}_{fs} and $\dot{\eta}^b_{\infty}$ should be zero, experimentally we observe that $\dot{\eta}^b$ is asymptotic and finite by $t \approx 0.3\ \mu$s, and it remains at this relative velocity for a duration on the order of 10 μs, in contradiction with Eq. 2.4. The predicted spike velocities, however, are within $\approx 20\%$ for both Sn experiments, but the comparisons between the measured and predicted bubble velocity terms is most consistent for the highest pressure Sn experiment, Sn-pRad0425 ($P_{SB} = 26.7$ GPa), than it is for the lower pressure Sn experiment, Sn-pRad0427 ($P_{SB} = 21.9$ GPa), especially at the smallest $\eta_0 k$ products which are the most relevant $\eta_0 k$ products for ejecta production from explosively shocked metals. This is probably related to the equation of state of Sn which releases to 100% solid for an initial stress of $P_{SB} \approx 19.5$ GPa, and which releases to 100% liquid for $P_{SB} \approx 33$ GPa (e.g., see Mabire & Hereil (1999); Greeff, Chisolm & George (2005)). The physics implies the ratio of solid-to-liquid metal is near one for the lower pressure experiment, i.e., even though the Sn is in a partial liquid state it retains some residual strength greater than simple surface tension, attenuating the bubble growth rates faster for the lower pressure Sn experiment ($P_{SB} = 21.9$ GPa) than for the higher pressure Sn experiment ($P_{SB} = 26.7$ GPa). For the lower pressure experiment the asymptotic bubble velocity $\dot{\eta}^b(t = 0.3\ \mu s)$ – relative to u^{∞}_{fs} – quickly approaches zero, whereas for the higher pressure experiment the bubble velocity is asymptotic and finite at late times (on the order of 10 μs).

Unsurprisingly, Eq. 2.4 does not predict well $\dot{\eta}^b$ for the Cu experiment, Cu-pRad0426. The Cu is 100% solid on shock and release. There is no reason to expect the Cu to plastically flow for an extended period of time to feed mass from the bubbles into the Cu spikes.

5. Strength at High-Strain and High-Strain Rate

In ejecta experiment Cu-pRad0426 velocimetry data were obtained on solid Richtmyer-Meshkov (RM) unstable 2D copper spikes. The analytical results of Piriz, Lopez-Cela & Tahir (2010) for the strains and strain rates in growing RM unstable perturbations, the Cu-pRad0426 data, and the standard PTW material strength model (see Preston et al. (2003)) are used to estimate the time dependence of the strain rate, temperature, and

flow stress in the growing spikes. Comparison with the Piriz expression for the yield stress shows a significant discrepancy.

Piriz, Lopez-Cela & Tahir (2010) have constructed an analytical model for the strength-limited RM unstable growth of sinusoidal 2D perturbations at the free surface of a solid. The modeled growth is initiated by a step function in the pressure at the solid-vacuum interface. This pressure discontinuity drives a shockwave into the solid from the initial vacuum region ($A \approx 1$), thus the RM-unstable solid perturbations grow on the shock Hugoniot of the solid. However, the flow stress of the solid reduces the growth rate and determines the maximum height – unbounded for a fluid – to which the perturbations grow. The model involves a single parameter that was determined by means of 2D numerical simulations. The constitutive behavior is taken to be elastic-perfectly plastic with yield strength Y. Their *generalized* model for the maximum spike height may be written

$$\frac{\eta_\infty^s - \eta_0}{\eta_0} = \mu\, \eta_0 k\, \frac{\rho\, u_p^2}{Y}\,, \tag{5.1}$$

where η_∞^s (η_0) is the maximum (initial) spike height, k is the perturbation wavenumber, ρ is the material density in the shock state, and u_p is the particle velocity. From 2D simulations the parameter μ was determined to equal 0.29.

Ejecta are formed when a shockwave propagates into the perturbations from within the solid, a rarefaction (release wave) reflects from the perturbations into the bulk solid, and the RM unstable spikes (perturbations) grow and breakup at zero pressure. These loading conditions differ fundamentally from those considered by Piriz *et al.* Nevertheless it is reasonable to assume that the maximum spike height is of the same form as Eq. 5.1 but with $u_p \to u_{fs}$, the free surface velocity, and $\rho \to \rho_0$, the ambient density

$$\frac{\eta_\infty^s - \eta_0}{\eta_0} = \eta_0 k\, \rho_0\, u_{fs}^2 \frac{\mu'}{Y}\,. \tag{5.2}$$

The coefficient, μ', may differ from $\mu = 0.29$ used in Eq. 5.1. A careful analysis, similar to that carried out by Piriz, Lopez-Cela & Tahir (2010), is needed to determine μ' for the loading conditions specific to ejecta formation. Equation 5.2 can be used to extract Y/μ' from the velocimetry data on pRad4026 for, in particular, $\eta_0 k = 0.35$ (Fig. 3), which exhibited arrested growth. Time integration of the measured $u_s - u_{fs}$ gives $\eta_\infty^s - \eta_0$ appearing in Eq. 5.2; we find $\eta_\infty^s - \eta_0 = 160$ μm. With $\eta_0 = 31$ μm, $\rho_0 = 8.93$ g/cm^3, and $u_{fs} = 1.46$ mm/μs, we obtain $Y = 12.9\,\mu'$ kbar. If we assume $\mu' = 0.29$ then $Y = 3.7$ kbar.

To see if this constant yield stress is physically reasonable, we will calculate the time dependence of the strain, strain rate, temperature, and flow stress during spike growth using the PTW constitutive model (see Preston et al. (2003)).

Let the solid occupy the negative half space $y \leqslant 0$ of an $x - y$ coordinate system. In the approximation that the solid is incompressible, the velocity field of the growing perturbations is of the form (Piriz, Lopez-Cela & Tahir 2010)

$$\begin{aligned} v_x &= \alpha^{-1}\, \dot{\eta}(t)\, \exp\left(k\, y\, /\, \alpha\right) \cos\left(k\, x\right), \\ v_y &= \dot{\eta}(t)\, \exp\left(k\, y\, /\, \alpha\right) \sin\left(k\, x\right). \end{aligned} \tag{5.3}$$

This single-mode model will provide only a crude approximation to the true strain rates, temperatures, and stresses when the strains in the spikes are large, as in Cu-pRad0426. The plastic strain rate tensor has the three independent components

$$\dot{\epsilon}_{xx} = \frac{\partial\, v_x}{\partial\, x},\ \dot{\epsilon}_{xy} = \frac{1}{2}\left(\frac{\partial\, v_x}{\partial\, y} + \frac{\partial\, v_y}{\partial\, x}\right),\ \dot{\epsilon}_{yy} = \frac{\partial\, v_y}{\partial\, y}. \tag{5.4}$$

The corresponding equivalent plastic strain rate is given by

$$\dot{\epsilon} = \left(\frac{2}{3}\,\dot{\epsilon}_{ij}\dot{\epsilon}_{ij}\right)^{1/2}$$
$$= \frac{1}{\sqrt{3}}\,k\,\dot{\eta}(t)\,\exp\left(k\,y\,/\,\alpha\right)\left\{\left(\frac{1}{\alpha^2}+1\right)^2 - \left(\frac{1}{\alpha^2}-1\right)^2 \sin^2\left(k\,x\right)\right\}^{1/2}, \qquad (5.5)$$

which can be simplified by noting that $\alpha^{-2} \approx 9$ (Piriz, Lopez-Cela & Tahir 2010), thus $\alpha^{-2} \pm 1 \approx \alpha^{-2}$

$$\dot{\epsilon} = \frac{1}{\alpha^2\sqrt{3}}\,k\,\dot{\eta}(t)\,\exp\left(ky/\alpha\right)|\cos\left(k\,x\right)|. \qquad (5.6)$$

We now calculate the average strain rate in the spikes as a function of time. The strain rate for $y = -\eta^b(t)$, i.e. at the bottoms of the bubbles, is proportional to $\exp\left(-\eta^b(t)k/\alpha\right)$, and therefore decreases exponentially with spike height† from its initial value $\exp\left(-\eta_0 k/\alpha\right)$, which $\approx \exp\left(-1\right)$ for Cu-pRad0426 with $\eta_0 = 31$ μm and $\lambda = 550$ μm; hence, the plastic flow below the bubbles can be neglected. We accordingly define the mean strain rate in the spikes by integrating from the bubbles to the spike tips

$$\langle\dot{\epsilon}(t)\rangle_{xy} = \frac{1}{\alpha^2\sqrt{3}}\,k\,\dot{\eta}(t)\frac{2}{\lambda}\frac{1}{2\eta(t)}\int_{-\lambda/4}^{\lambda/4} dx \int_{-\eta(t)}^{\eta(t)\,\sin(k\,x)} dy\, e^{k\,y/\alpha}\,\cos\left(k\,x\right)$$
$$= \frac{\dot{\eta}(t)}{\alpha\sqrt{3}\,\pi\,\eta(t)}\left[\frac{\alpha}{\eta(t)\,k}\,\sinh\left(\frac{\eta(t)\,k}{\alpha}\right) - \exp\left(\frac{\eta(t)\,k}{\alpha}\right)\right]. \qquad (5.7)$$

The spike height is a quadratic function of the time (Piriz, Lopez-Cela & Tahir 2010)

$$\eta(t) = \eta_0 + \dot{\eta}_0\,t\left(1 - \frac{t}{2\,t_m}\right), \qquad (5.8)$$

where t_m, the time when the spikes reach their maximum height, is given by

$$t_m = \frac{2\,(\eta^s_\infty - \eta_0)}{\dot{\eta}_0}. \qquad (5.9)$$

From the velocimetry data for Cu-pRad0426, $\eta_0 k = 0.35$, we determine that $\eta^s_\infty - \eta_0 = 160$ μm and $\dot{\eta}_0 = u^s_{pk} - u_{fs} = (2.15 - 1.46)$ mm/μs$= 690$ μm/μs, which gives $t_m = 0.46$ μs. The spike tip velocity follows from Eq. 5.8

$$\dot{\eta}(t) = \dot{\eta}_0\left(1 - \frac{t}{t_m}\right). \qquad (5.10)$$

Substitution of Eqs. 5.8 and 5.10 into Eq. 5.7 yields the time dependence of the mean plastic strain rate in the spikes (see Fig. 4(a)). Averaging $\langle\dot{\epsilon}(t)\rangle_{xy}$ over time gives $\langle\dot{\epsilon}\rangle_{xyt} = 1.5 \times 10^7$/s.

The mean plastic strain as a function of time is

$$\langle\epsilon(t)\rangle_{xy} = \int_0^t dt'\,\langle\dot{\epsilon}(t')\rangle_{xy} = \frac{1}{\alpha\sqrt{3}\,\pi}\left[f\left(\frac{\eta(t)\,k}{\alpha}\right) - f\left(\frac{\eta_0\,k}{\alpha}\right)\right], \qquad (5.11)$$

where

$$f(x) = \frac{1}{2}\left[Ei\left(x\right) - Ei\left(-x\right)\right] - \frac{\sinh(x)}{x}. \qquad (5.12)$$

† In Piriz, Lopez-Cela & Tahir (2010) the main assumption is that $\eta^s = \eta^b = \eta$ in their single-mode model.

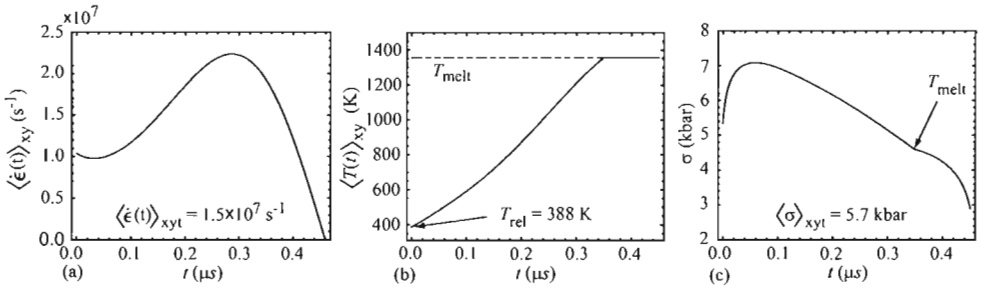

FIGURE 4. Cu-pRad 0426, $\eta_0 k = 0.35$, $P_{SB} \approx 36$ GPa. (a) Mean plastic strain rate in the Cu spikes vs. time. (b) The mean Cu spike temperature vs time. The temperature reaches $T_{melt} \approx 1300$ K at 0.35 μs, but the Cu remains solid until growth arrest at 0.46 μs. (c) Time dependence of the mean stress in the Cu spikes.

The mean plastic strain in Cu-pRad0426, $\eta_0 k = 0.35$, increases monotonically from zero to approximately 700%.

The shock pressure for Cu-pRad0426 was 36.1 GPa. A new copper two-phase equation of state constructed by one of us (DLP) gives the corresponding shock release temperature as 388 K, assuming an initial temperature of 293 K. In addition to this 95 K rise in temperature following shock release, the temperature will continue to rise in the growing spikes because of the adiabatic heating due to plastic work

$$\Delta T(\epsilon) = \frac{1}{\rho_0 C_p} \int_0^{\epsilon} \sigma(\epsilon, \dot{\epsilon}, T(\epsilon), P = 0)\, d\epsilon. \tag{5.13}$$

Here σ is the flow stress (yield stress is the flow-stress at zero strain), and C_p is the specific heat. A reasonable definition of the mean spike temperature is provided by

$$\frac{d\,\langle T(t)\rangle_{xy}}{dt} = \frac{1}{\rho_0 C_p}\, \sigma(\langle\epsilon(t)\rangle_{xy}, \langle\dot{\epsilon}(t)\rangle_{xy}, \langle T(t)\rangle_{xy}, P = 0)\, \langle\dot{\epsilon}(t)\rangle_{xy}. \tag{5.14}$$

This first-order, non-linear ODE was solved numerically for the PTW model of the flow stress, σ. The solution is shown in Fig. 4(b).

The mean temperature of the spikes reaches the melting temperature at 0.35 μs ($\langle\epsilon\rangle_{xy} = 5.7$). The plastic work from this time to growth arrest at 0.46 μs ($\langle\epsilon\rangle_{xy} = 6.9$) is ≈ 4 kbar $\times(6.9 - 5.7) = 4.8 \times 10^9$ erg/cm^3, which is $\approx 25\%$ of the heat required to melt the copper (latent heat $= 1.8 \times 10^{10}$ erg/cm^3); hence, neglecting localized melting, the copper remains solid up to growth arrest.

In Fig. 4(c) we plot $\sigma(\langle\epsilon(t)\rangle_{xy}, \langle\dot{\epsilon}(t)\rangle_{xy}, \langle T(t)\rangle_{xy}, P = 0)$. The figure clearly shows that the spike growth becomes plastically unstable at $t = 0.06$ μs, which corresponds to a strain of $\epsilon \approx 60\%$. The time- and spatially-averaged PTW flow stress is found to be 5.7 kbar, which is 54% higher than the value $Y = 3.7$ kbar predicted by Eq. 2.10 ($\mu' = 0.29$ in Eq. 5.2).

The simple constitutive relation chosen in Piriz, Lopez-Cela & Tahir (2010), namely elastic-perfectly plastic with a constant Y, is a poor approximation to the actual constitutive behavior, as shown in our case in Fig. 4. In order to extract high strain rate flow stresses from ejecta data it will be necessary to generalize Eq. 5.2 using a more realistic constitutive relation.

6. Conclusions

Much work remains to be done along the lines of ejecta model development, but our work with a simple Mikaelian model demonstrates that the supposition that ejecta form as a limiting case of a RM model is well founded. Using such a model we have successfully demonstrated that spike velocities $\dot{\eta}^s_\infty$ are predicted within $\lesssim 20\%$ of observed, measured velocities for wavenumber and amplitude products up to $\eta_0 k = 2$. The basic model was less successful predicting the bubble velocities $\dot{\eta}^b(t)$ at early or late times, even though it is thought that the bubble velocity physics are better understood (in our ejecta studies we assume that the bubble heights relate to the total amount of ejected mass from the perturbations). The failure to predict well the bubble velocities is a surprise, but most RM instability studies focus on two fluid mixing, and these data present an opportunity to study RM physics of liquid metals in the limiting extreme of $A = -1$.

Observation of the spike rise-times is also of interest because of differences seen between mass ejected in flyer plate experiments as compared with mass ejected in our small scale HE experiments. We surmised that perhaps in ejecta experiments driven by unsupported shockwaves, that as the material releases into tension the physical property that feeds ejecta mass into unstable growth is somehow quickly stopped. This phenomena is observed in our small scale experiments where the ejected masses become asymptotic with increasing pressure for HE experiments that are liquid on release, but the ejected mass appears to linearly increase with pressure for supported shockwave experiments at similar peak loading pressures (Buttler & Zellner 2011).

The Eq. 2.10 relation, or more generally Eq. 5.1, for RM unstable spike growth was suggested by the result of Piriz, Lopez-Cela & Tahir (2010) for step-function pressure loading of the interface where the Atwood number is $A = 1$. In order to extract the plastic constitutive properties/parameters of real materials from velocimetry data, an analogous relation must be derived for the loading conditions specific to ejecta formation and for a realistic constitutive relation accounting for work hardening, strain rate sensitivity, and temperature dependence; this will be the focus of our future theoretical work. With such a relation at hand we would be able to determine large-strain flow stresses at plastic strain rates greater than or of order 10^7/s on well-characterized metals and alloys. This would be a unique capability: there is presently no technique for reliably measuring flow stresses at strain rates above 10^6/s. In addition, the theory of plastic flow at these deformation rates is particularly challenging because the dislocation glide is controlled by both thermally-activated intersection and dislocation drag mechanisms. This new technique would provide data that are essential for the construction of constitutive relations applicable at strain rates greater than 10^6/s.

This work sets the stage for improvements to ejecta transport studies. While we have collected initial transport data, data from similarly well controlled experiments as these are important for validation of current elements of our hydrodynamic transport models.

This work was supported by the United States Department of Energy under the auspices of the Science Campaigns, especially Campaign 1, Campaign 2, and the Physics and Engineering Models Campaign.

We acknowledge the support of the pRad team to acquire these data, especially J. R. Bainbridge, G. E. Hogan, B. Hollander, K. Kwiatkowski, M. Marr-Lyon, F. Mariam, F. E. Merrill, P. Nedrow, A. Saunders, and W. S. Vogan-McNeil. In addition, we appreciate contributions to these experiments by members of the LANL MST-7 group where our Sn and Cu targets were machined and characterized by Felix Garcia, Bob Day and Derek Schmidt.

William T. Buttler thanks B. J. Balakumar for helpful discussions on the topics of instability physics.

Lastly, William Buttler acknowledges the longtime support of Molly Moore.

REFERENCES

BOURNE, N. K. & AND GRAY, G. T., III 2005a Computational design of recovery experiments for ductile materials. *Proc. Royal Soc. A* **461**, 3297–3313.

BOURNE, N. K. & AND GRAY, G. T., III. 2005b Soft-recovery of shocked polymers and composites. *J. Phys. D: Appl. Phys.* **38**, 3690–3694.

BUTTLER, W. T., LAMOREAUX, S. K., OMENETTO, F. G. & TORGERSON, J. R. 2004 Optical velocimetry. arXiv:physics/0409073v1.

BUTTLER, W. T., ZELLNER, M. B., OLSON, R. T., RIGG, P. A., HIXSON, R. S., HAMMERBERG, J. E., OBST, A. W., PAYTON, J. R., IVERSON, A. & YOUNG, J. 2007a Dynamic comparisons of piezoelectric ejecta diagnostics. *J. Appl. Phys.* **101**, 063547.

BUTTLER, W. T., ROUTLEY, N., HIXSON, R. S., KING, N. S. P., OLSON, R. T., RIGG, P. A., RIMMER, A. & ZELLNER, M. B. 2007b Method to separate and determine the amount of ejecta produced in a second material-fragmentation event. *Appl. Phys. Lett.* **90**, 151921.

BUTTLER, W. T. & ZELLNER, M. B. 2007 Tin ejecta data review: toward a statistical material fragmentation model, Milestone 2478. *Tech. Rep.* LA-UR-07-6522. Los Alamos National Laboratory.

BUTTLER, W. T. & ZELLNER, M. B. Unpublished results gathered between 2005 and 2011.

DIMONTE, G. & RAMAPRABHU, R. 2010 Simulations and model of the nonlinear Richtmyer-Meshkov instability. *Phys. Fluids* **22**, 014104.

FORMAN, JR., J. W., GEORGE, E. W. & LEWIS, R. D. 1965 Feasibility study of a laser flowmeter for local velocity measurements in gas flow fields. *Tech. Rep.* Tech. Note #149, Teledyne Brown Engineering Co. Inc., Huntsville, AL.

FORMAN, JR., J. W., GEORGE, E. W. & LEWIS, R. D. 1965 Measurement of localized fluid flow velocities in gasses with a laser Doppler flowmeter. *Appl. Phys. Lett.* **7**, 77–78.

GREEFF, C., CHISOLM, E. & GEORGE, D. 2005 SESAME 2161: An explicit multiphase equation of stte for tin. *Tech. Rep.* LA-UR-05-9414. Los Alamos National Laboratory.

MABIRE, C. & HEREIL, P. L. 1999 Shock induced polymorphic transition and melting of tin up to 53 GPa (experimental study and modelling). *AIP Conf. Proc.* **505**, 93–96.

MESHKOV, E. E. 1969 Instability in shock-accelerated boundary separating two gasses. *Izv. Akad. Nauk SSSR, Mekh. Zhidk. Gasa* **5**, 151–158.

MEYER, K. A. & BLEWETT, P. J. 1972 Numerical investigation of the stability of a shock-accelerated interface between two fluids. *Phys. Fluids* **15**, 753–759.

MIKAELIAN, K. O. 1998 Analytical approach to nonlinear Rayleigh-Taylor and Richtmyer-Meshkov instabilities. *Phys. Rev. Lett.* **80**, 508–511.

MIKAELIAN, K. O. 2010 Analytical approach to nonlinear hydrodynamic instabilities driven by time-dependent accelerations. *Phys. Rev. E* **81**, 016325.

PIRIZ, A. R., LOPEZ-CELA, J. J. & TAHIR, N. A. 2010 Richtmyer-Meshkov instability as a tool for evaluating material strength under extreme conditions. *Nucl. Instrum. Meth. Phys. Res. A* **606**, 139–141.

PRESTON, D. L., TONKS, D. L. & WALLACE, D. C. 2003 Model of plastic deformations for extreme loading conditions. *J. Appl. Phys.* **93**, 211–220.

RICHTMYER, R. D. 1960 Taylor instability in shock acceleration of compressible fluids. *Commun. Pure Appl. Math* **13**, 297–319.

STRAND, O. T., GOOSMAN, D. R., MARTINEZ, C. & WHITWORTH, R. L. 2006 Compact system for high-speed velocimetry using heterodyne techniques. *Rev. Sci. Instrum.* **77**, 083108.

VELIKOVICH, A. L. & DIMONTE, G. 1996 Nonlinear perturbation theory of the incompressible Richtmyer-Meshkov instability. *Phys. Rev. Lett.* **76**, 3112–3115.

VOGAN, W. S., ANDERSON, W. W., GROVER, M., HAMMERBERG, J. E., KING, N. S. P., LAMOREAUX, S. K., MACRUM, G., MORLEY, K. B., RIGG, P. A., STEVENS, G. D., TURLEY, D., VEESER, L. R. & BUTTLER, W. T. 2005 Piezoelectric characterization of ejecta from shocked tin surfaces. *J. Appl. Phys.* **98**, 113508.

YEH, Y. & CUMMINS, H. Z. 1964 Localized fluid flow measurements with an He-Ne laser. *App. Phys. Lett.* **4**, 176–178.

ZELLNER, M. B., GROVER, M., HAMMERBERG, J. E., HIXSON, R. S., IVERSON, A. J., MACRUM, G. S., MORLEY, K. B., OBST, A. W., OLSON, R. T., PAYTON, J. R., RIGG, P. A., ROUTLEY, N., STEVENS, G. D., TURLEY, W. D., VEESER, L. & BUTTLER, W. T. 2007 Effects of shock breakout pressure on ejection of material from shocked tin surfaces. *J. Appl. Phys.* **102**, 013522.

ZELLNER, M. B., VOGAN-MCNEIL, W., GRAY, G. T., III, HUERTA, D. C., KING, N. S. P., NEAL, G. E., VALENTINE, S. J., PAYTON, J. R., RUBIN, J., STEVENS, G. D., TURLEY, W. D., & BUTTLER, W. T. 2008 Surface preparation methods to enhance dynamic surface property measurements of shocked metal surfaces. *J. Appl. Phys.* **103**, 083521.

ZELLNER, M. B., GROVER, M., HAMMERBERG, J. E., HIXSON, R. S., IVERSON, A. J., MACRUM, G. S., MORLEY, K. B., OBST, A. W., OLSON, R. T., PAYTON, J. R., RIGG, P. A., ROUTLEY, N., STEVENS, G. D., TURLEY, W. D., VEESER, L. & BUTTLER, W. T. 2008 Erratum: Effects of shock-breakout pressure on ejection of material from shocked tin surfaces [(2007) *J. Appl. Phys.* **102**, 013522]. *J. Appl. Phys.* **103**, 109901.

ZELLNER, M. B., VOGAN-MCNEIL, W., HAMMERBERG, J. E., HIXSON, R. S., OBST, A. W., OLSON, R. T., PAYTON, J. R., RIGG, P. A., ROUTLEY, N., STEVENS, G. D., TURLEY, W. D., VEESER, L. & BUTTLER, W. T. 2008 Probing the underlying physics of ejecta production from shocked Sn samples. *J. Appl. Phys.* **103**, 123502.

ZELLNER, M. B. & BUTTLER, W. T. 2008 Exploring Richtmyer-Meshkov instability phenomena and ejecta cloud physics. *Appl. Phys. Lett.* **93**, 114102.

ZHANG, Q. 1998 Analytical solution of Layzer-type approach to unsatable interfacial fluid mixing. *Phys. Rev. Lett.* **81**, 3391–3394.

Appendix A

The images that follow present the full set of Sn and Cu data from Sn-pRad0425, Cu-pRad0426, and Sn-pRad0427. The data include the proton radiographs in the upper portion of the figures (the (a) images), with time stamps relative to shockwave breakout at the metal-vacuum interface positioned above the images, showing the time of each radiograph. The (b) image presents the LDV data for the perturbation regions. Sn-pRad0425 is seen in Fig. 5, Cu-pRad0426 in Fig. 6, and Sn-pRad0427 in Fig. 7. For all images the wavelength of the perturbations is $\lambda = 0.55$ mm, and the units of all velocimetry is millimeters per microsecond.

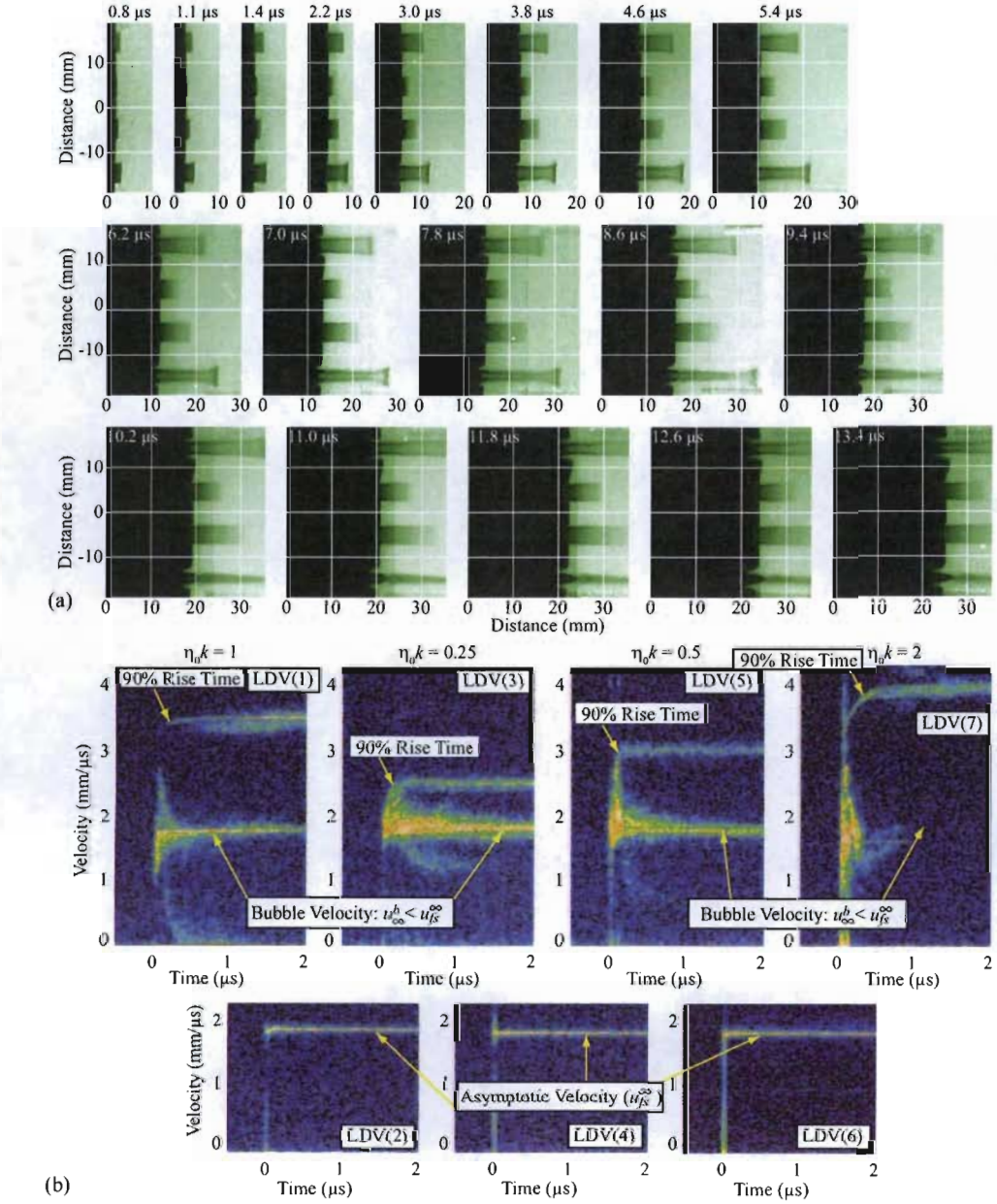

FIGURE 5. Full set of Sn-pRad0425 *cropped* proton radiographs. The time of each radiograph relative to shockwave breakout at the free-surface is seen just above each image. The units of the horizontal and vertical axes are millimeters. The largest $\eta_0 k$ wavenumbers have the largest, and the smallest wavenumbers the lowest $\dot{\eta}_\infty^s$. From top to bottom, we have $\eta_0 k \in \{1.0, 0.25, 0.5, 2.0\}$, as shown in Fig. 2.

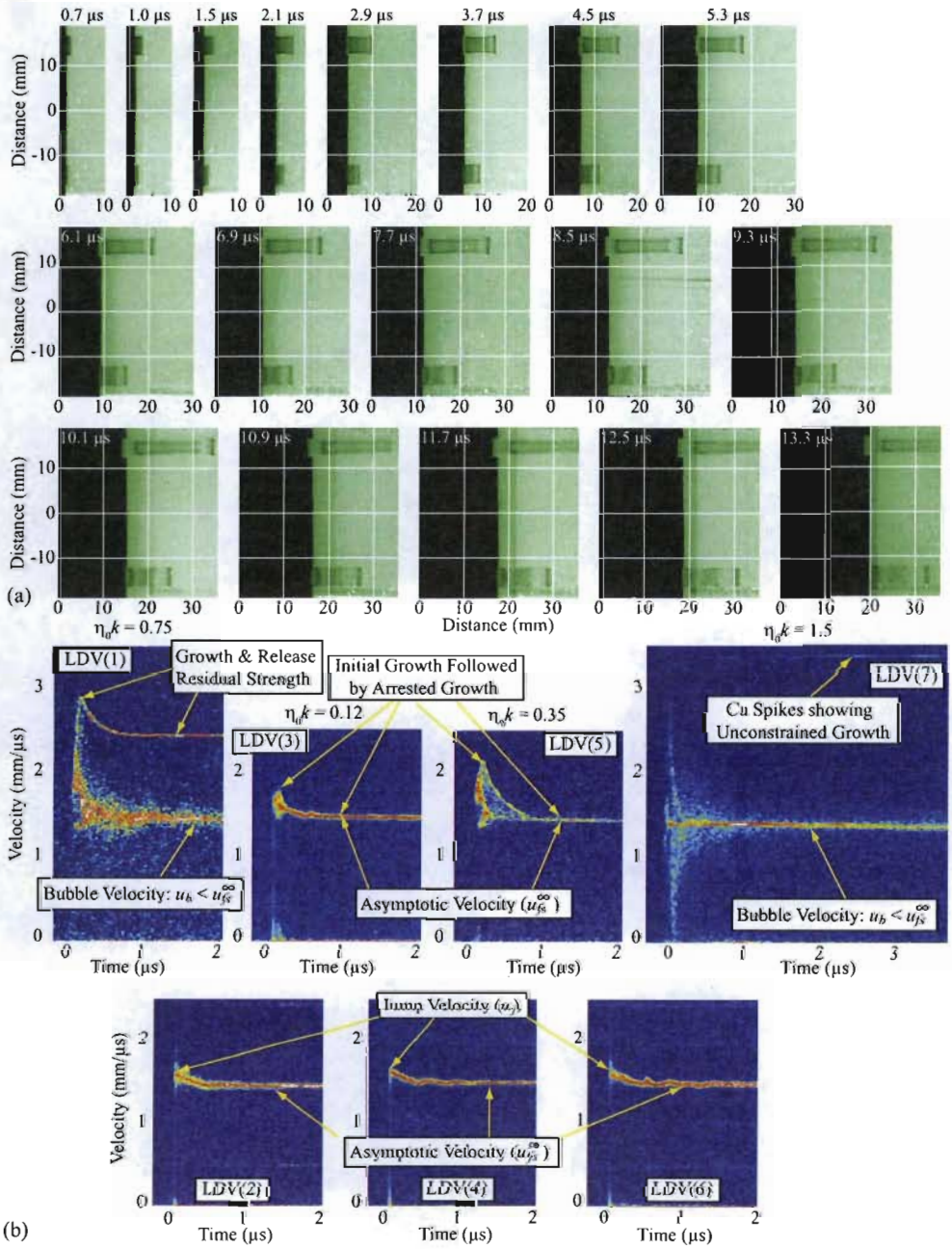

FIGURE 6. Full set of Cu-pRad0426 *cropped* proton radiographs. The time of each radiograph relative to shockwave breakout at the free-surface is seen just above each image. The units of the horizontal and vertical axes are millimeters. The largest $\eta_0 k$ wavenumbers have the largest, and the smallest wavenumbers the lowest $\dot{\eta}_\infty^s$. From top to bottom, we have $\eta_0 k \in \{0.75, 0.12, 0.35, 1.5\}$, as shown in Fig. 2.

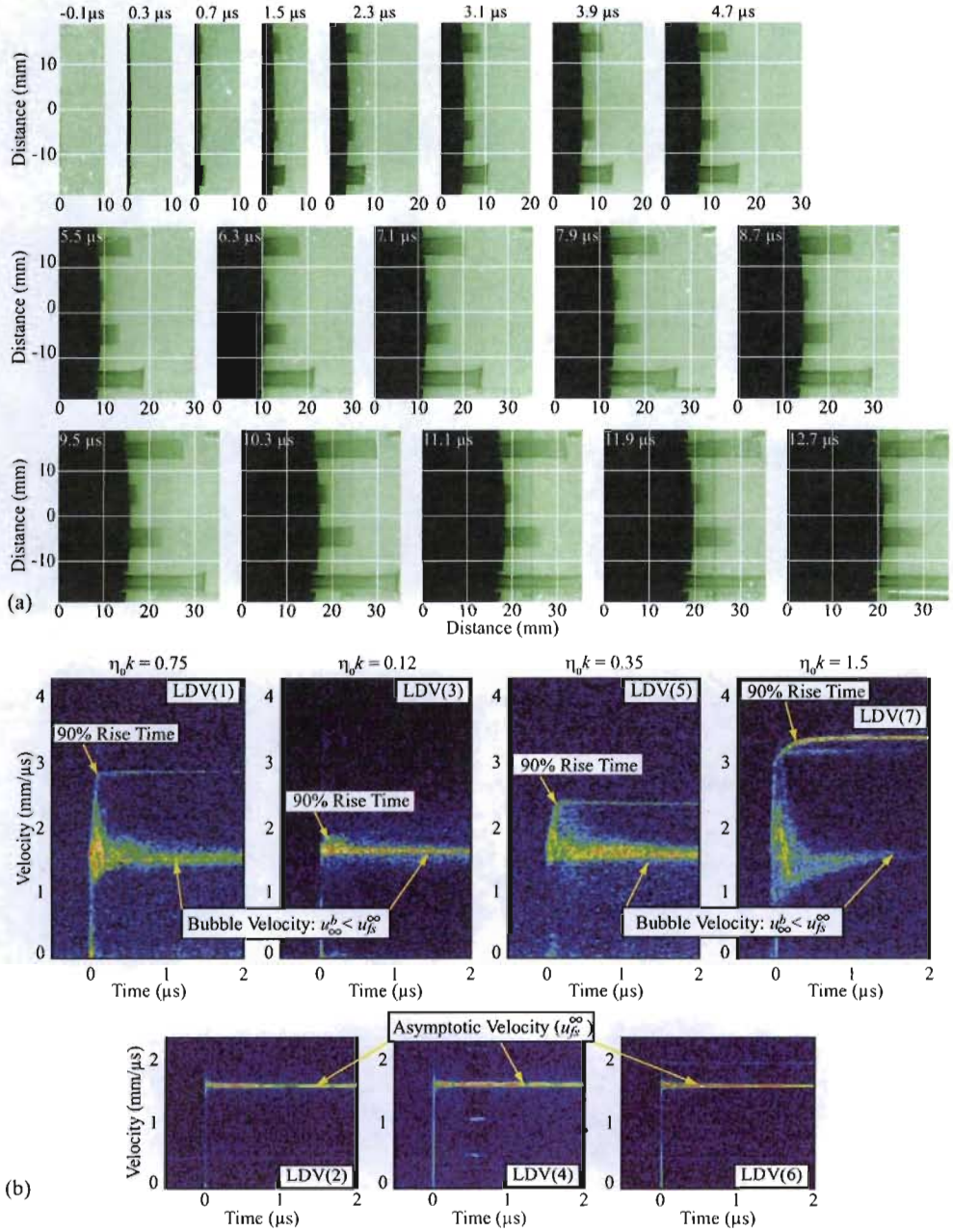

FIGURE 7. Full set of Sn-pRad0427 *cropped* proton radiographs. The time of each radiograph relative to shockwave breakout at the free-surface is seen just above each image. The units of the horizontal and vertical axes are millimeters. The largest $\eta_0 k$ wavenumbers have the largest, and the smallest wavenumbers the lowest $\dot{\eta}_\infty^s$. From top to bottom, we have $\eta_0 k \in \{0.75, 0.12, 0.35, 1.5\}$, as shown in Fig. 2.